Behavioral/Cognitive

Distinct Progressions of Neuronal Activity Changes Underlie the Formation and Consolidation of a Gustatory Associative Memory

Elor Arieli,[1] Nadia Younis,[1] and Anan Moran[1,2]

[1]Department of Neurobiology, The School of Neurobiology, Biochemistry and Biophysics, The George S. Wise Faculty of Life Science, Tel Aviv University, Tel Aviv 6997801, Israel, and [2]Sagol School of Neuroscience, Tel Aviv University, Tel Aviv 6997801, Israel

Acquiring new memories is a multistage process. Numerous studies have convincingly demonstrated that initially acquired memories are labile and are stabilized only by later consolidation processes. These multiple phases of memory formation are known to involve modification of both cellular excitability and synaptic connectivity, which in turn change neuronal activity at both the single neuron and ensemble levels. However, the specific mapping between the known phases of memory and the changes in neuronal activity at different organizational levels—the single-neuron, population representations, and ensemble-state dynamics—remains unknown. Here we address this issue in the context of conditioned taste aversion learning by continuously tracking gustatory cortex neuronal taste responses in alert male and female rats during the 24 h following a taste–malaise pairing. We found that the progression of activity changes depends on the neuronal organizational level: whereas the population response changed continuously, the population mean response amplitude and the number of taste-responsive neurons only increased during the acquisition and consolidation phases. In addition, the known quickening of the ensemble-state dynamics associated with the faster rejection of harmful foods appeared only after consolidation. Overall, these results demonstrate how complex dynamics in the different representational levels of cortical activity underlie the formation and stabilization of memory within the cortex.

Key words: **conditioned taste aversion; ensemble activity; learning; neuronal coding; neuronal dynamics; Consolidation**

Significance Statement

Memory formation is a multiphased process; early acquired memories are labile and consolidate to their stable forms over hours and days. The progression of memory is assumed to be supported by changes in neuronal activity, but the mapping between memory phases and neuronal activity changes remains elusive. Here we tracked cortical neuronal activity over 24 h as rats acquired and consolidated a taste–malaise association memory, and found specific differences between the progression at the single-neuron and populations levels. These results demonstrate how balanced changes on the single-neuron level lead to changes in the network-level representation and dynamics required for the stabilization of memories.

Introduction

Learning is not a discrete event, but rather an evolving process (Bailey and Kandel, 1993; Dudai, 2004; Aceti et al., 2015; Klinzing et al., 2019). More than a century of human and animal research has identified several key phases in the progression of memory formation (Müller and Pilzecker, 1900; Dudai, 2004; Klinzing et al., 2019; Haubrich et al., 2020) including the following: (1) the acquisition of an initial, labile memory which is protein synthesis independent; and (2) the consolidation and stabilization of the memory through a process that does require protein synthesis. The transition between these two phases has mainly been studied using hippocampus-dependent learning paradigms in which the acquisition-to-consolidation dynamic reflects the transfer of the memory from the hippocampus to the cortex (Squire and Alvarez, 1995; Buzsáki, 1996; Eichenbaum, 2000). It is unclear, however, how this two-stage process plays out in nonhippocampal forms of learning.

Conditioned taste aversion (CTA; Garcia et al., 1955) is a hippocampal-independent classical conditioning paradigm in which a novel taste becomes aversive after pairing it with malaise. Although subserved by various brain regions, the gustatory cortex (GC) was shown to play a major part during the formation of

Received Aug. 5, 2021; revised Oct. 24, 2021; accepted Nov. 21, 2021.

Author contributions: E.A. and A.M. designed research; E.A. and N.Y. performed research; E.A. analyzed data; E.A. and A.M. wrote the paper.

This research was partially supported by the Israel Science Foundation (Grant 2895/20), the Colton Foundation (A.M.), and a seed grant from the Tel Aviv University.

The authors declare no competing financial interests.

Correspondence should be addressed to Anan Moran at anan@tauex.tau.ac.il.

https://doi.org/10.1523/JNEUROSCI.1599-21.2021

CTA. Importantly, biochemical studies of the GC during CTA have identified two distinct memory phases in the hours after training: an acquisition phase that takes place during the first ~3 post-training hours (Rosenblum et al., 1993; Ferreira et al., 2002; Moguel-González et al., 2008) and a consolidation phase that occurs 5–7 h post-training (Ferreira et al., 2002; Ma et al., 2011; Martínez-Moreno et al., 2011; Xin et al., 2014).

The molecular pathways that underlie the formation and consolidation of memories act, at least in part, to change the synaptic strength between neurons (Aizenman et al., 2000; Bi and Poo, 2001; Dudai, 2002; Tye et al., 2008), which hence change the firing rates (FRs) of the postsynaptic neurons (and crucially, the rates in response to taste stimuli), a change that is believed to constitute the memory itself and drive the learning-induced behavioral change. Given the presumed "instability" in neuronal activity before complete consolidation, researchers have typically tended to wait at least 24 h before testing for more stable learning-related activity changes (Grossman et al., 2008; Moran and Katz, 2014). Twenty-four hours after CTA induction, GC neuronal activity was indeed reported to show firing-rate modulations (Yamamoto and Fujimoto, 1991; Yasoshima and Yamamoto, 1998; Moran and Katz, 2014). However, not all neuronal organizational levels showed similar fidelity with these behavior changes: whereas single-neuron response changes were poor predictors of the behavioral change, the neuronal population dynamics matched behavior across CTA acquisition and extinction (Moran and Katz, 2014). These differences are consistent with current theories arguing that interneuronal connectivity constrains the network activity to a low-dimensional manifold (Yu et al., 2009; Okun et al., 2015) constituting various patterns of network activation that process sensory information and drive behavior. In this framework, different sets of single-neuronal responses may yield similar network dynamics, and changes at the single-neuron level may not be directly mapped to network behavior. Whether the changes in the single-neuron and population level are mapped to some memory phases remains unknown.

Here we addressed this issue by continuously monitoring GC neuronal basal and taste-evoked activity in behaving rats before and after CTA training. We analyzed the activity of single neurons, communal population taste representations, and ensemble-state dynamics across acquisition and consolidation and found they have distinct progression profiles. Single GC neurons frequently changed their responsiveness to the conditioned taste in no apparent order, but these changes were balanced to produce a magnitude increase in the population taste response during the acquisition and consolidation phases. Interestingly, the known quickening of the ensemble-state dynamics only appears after the consolidation phase. These results are illustrative of the complex interactions between the different organizational levels of the GC whose distinct progression over time underlies the formation of a CTA memory.

Materials and Methods

Animals

Male ($n = 9$) and female ($n = 5$) Long–Evans adult rats (age, 3–4 months; weight, ~250 g) were raised in groups of two to four same-sex littermates in a 12 h light/dark cycle. The experiments were performed in the light portion of the cycle. Unless otherwise specified, the rats had *ad libitum* access to chow and water. Rats were handled for 15 min/d for 3 d before the experiments to habituate them to human touch and reduce stress. All methods and experiments conducted in this study comply with the Tel Aviv University Institutional Animal Care and Use Committee guidelines. All efforts were made to minimize animal suffering.

Surgery and postsurgery care

Anesthesia. Rats were temporarily anesthetized with isoflurane (0.5 ml/300 g) in an induction box, followed by an intraperitoneal injection of ketamine-xylazine (KX; 100 and 10 mg/kg, respectively; 1 ml/250 g). Supplemental intraperitoneal injections (one-third of the induction dose) were administered as needed.

Surgery. The anesthetized rat was placed in a stereotaxic frame and its scalp was excised, and holes were bored in its skull for the insertion of self-tapping ground screws. A craniotomy hole was drilled above the GC (AP = 1.4 mm, ML = 5 mm, relative to bregma), and the dura was removed. A self-manufactured electrode with a microdrive (Piette et al., 2012; Moran and Katz, 2014) was inserted into the brain and positioned 0.5 mm above the taste cortex (DV = −4.5 from dura). In addition, two intraoral cannulas (IOCs; flexible plastic tubing, AM-Systems) were inserted bilaterally through the oral cavity lateral to the second molar tooth (Phillips and Norgren, 1970). The entire structure composed of the electrode and the IOCs was covered with dental acrylic.

Postoperative treatment. Following surgery, the rats were given subcutaneous injections of antibiotics (5 mg/kg Baytril 5%), pain relievers (1 mg/kg Meloxicam 0.5%) and saline (10 ml/kg) to ensure hydration. The head wound margins were treated with antibiotic cream. Following surgery, the rats were single housed for 7 d in new cages and given wetted food pallets to help with recovery. Their weight was monitored to ensure proper recovery. During the recovery days, the electrodes were advanced periodically for a total of 1 mm, so that the entire electrode bundle resided within the GC.

Experimental design

The experimental procedure is illustrated in Figure 1*A*. After recovery, rats were put of the experimental group (Exp) chamber with *ad libitum* water for 3 d of acclimation (Acc) to the new environment. Food was always available throughout the experiment. On day 4, the rats were connected to the recording and taste delivery systems through a self-made dual commutator that provided uninterrupted, tangle-free, taste deliveries and electrophysiological signals (Fig. 1*B*; see detailed information below). During days 4–6, the rats were habituated to drink water from two bottles for 20 min in the morning, and then receive 10 drops of water (40 µl; 15 s between deliveries) through the IOC once every 2 h. At 9:00 A.M. of the seventh day ("training"), saccharin (Sac; 0.15% w/v) solution replaced water in the bottles that were provided for 20 min. At the end of the drinking session, pre-CTA neuronal activity was recorded during three IOC delivery sessions (~20 min intersession interval, 10 drops/session). Immediately after the third delivery session, the rats were subcutaneously injected with LiCl (0.3 M, 1% body weight) to induce gastrointestinal malaise. Following CTA induction, the protocol changed such that each liquid delivery session contained 5 drops of Sac and 10 drops of water, delivered randomly. The low number of Sac trials within a larger number of water trials was designed to reduce optional extinction effects, while still providing sufficient data for neuronal response analyses. These liquid delivery sessions were given twice during the first hour, then once every hour for 2 h and then once every 2 h until 4:00 A.M. The initial higher rate of taste sessions was aimed to test for more rapid changes in the short acquisition phase. Between 4 and 10 A.M. on the eighth day, the rats had no access to liquids to increase motivation to drink on the following CTA test. At 10:00 A.M. on the eighth day, the rats were given a two-bottle test with water and 0.15% Sac for 20 min. The level of learning was measured by calculating the aversion ratio, which was defined as the consumption of water divided by the total amount of liquids consumed (Sac and water), as follows:

$$\text{Aversion ratio} = \frac{\text{Water consumption}}{\text{Total consumption}}.$$

To control for LiCl and passage-of-time effects, we ran another group of rats that were familiarized (Fam) with the to-be-conditioned Sac taste during the 3 habituation days, provided in both the bottles and the IOC deliveries (Fig. 1*A*, Fam habituation). This repeated and prolonged exposure with the Sac taste interfered with later CTA learning [a latent inhibition (LI) effect; Lubow, 1973]. Importantly, apart from the

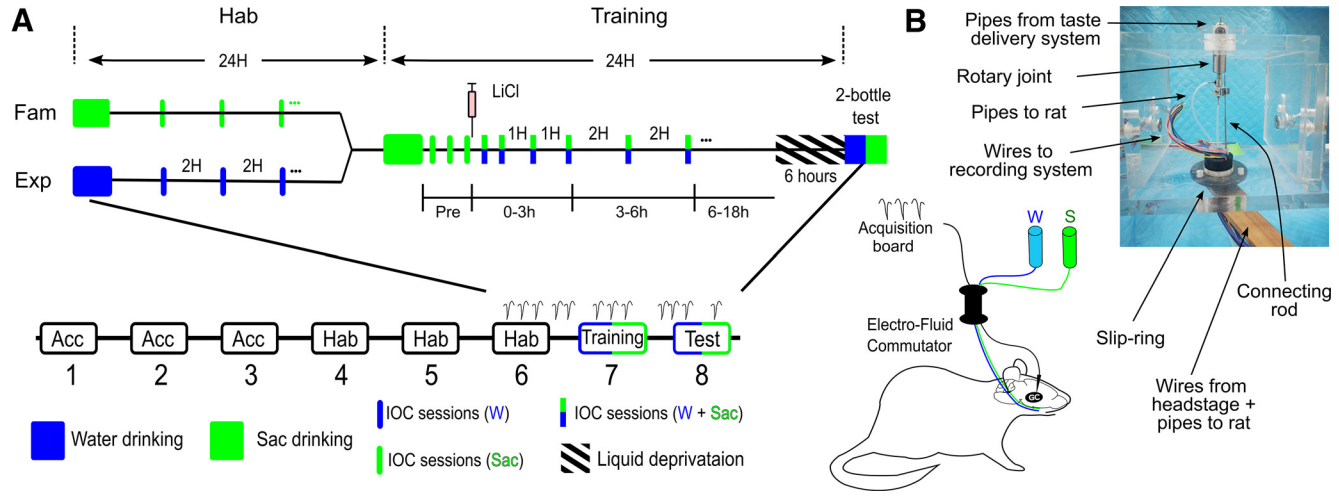

Figure 1. Experimental protocol and setup. ***A***, Experimental protocol. The rats were first acclimated (Acc) to the new environment with *ad libitum* food and water (days 1–3) and then habituated (Hab) to a watering regimen for 3 d (drinking water from bottles in the morning followed by IOC deliveries every 2 h). On day 7 (training), the rats received CTA, with periodic fluid stimulation at increasing intervals. Eighteen hours after training, IOC deliveries halted for 6 h. On the eighth day, rats underwent a two-bottle test (one with Sac, the other with water) to evaluate taste aversion. Rats in the Fam control group went through the same protocol but received Sac in the bottles and IOC deliveries during the Hab days. ***B***, Bottom, left, Illustration of a rat connected to the electro-fluid commutator that provided uninterrupted, tangle-free, neuronal activity recording and fluid deliveries. Top right, A picture of the electro-fluid commutator with its component parts. The rotary joint positioned on top and the bottom slip ring rotate together via the metal connecting rod. W, Water; S, Saccharin.

habituation phase, both the Exp group and the Fam control group went through the exact protocol of CTA training and testing. This design diminished the need to control for activity changes due to the passage of time, which is commonly done by injecting the rats with saline instead of LiCl. In other words, any such changes, if they occurred, would thus be similar in the Exp and Fam groups, and therefore disregarded.

Electro-fluid dual commutator

The dual commutator was built from a dual-channel liquid metal rotary joint (model ITH-375/D/20, Instech) and a 12-channel through-bore slip ring with a 5 mm hole (model SNH005-12, Senring; Fig. 1*B*). The rotary joint was held above the slip ring using a Perspex construction. The two commutators were connected with a metal rod, such that they rotated together. The tubes leaving the rotary joint passed through the hole in the slip ring and connected to thinner pipes that passed through the IOC to the oral cavity of the rat. The 12 wires of the slip ring were soldered to the 12 wires of the serial peripheral interface (SPI) interface cables. The SPI cable was protected by a metal spring to prevent damage by the rat. Both the cable and the tubes were affixed to a thin, 10-cm-long, wooden plank that was horizontally glued to the bottom of the slip ring to increase the torque.

Acquisition and analysis of electrophysiological data

For acquisition and preprocessing, extracellular neuronal signals were collected from self-manufactured 32-wire electrodes (0.0015 inch formvar-coated nichrome wire; A-M Systems) positioned within the GC (Piette et al., 2012; Moran and Katz, 2014). The data were first collected by an analog-to-digital headstage amplifier (model RHD2132, Intan Technologies) and then sampled at 30 kHz by an acquisition system (model RHD2000, Intan Technologies) and stored offline. Common noise was removed from each recorded channel using a common average reference algorithm. Automatic spike sorting was first performed using the KlustaKwik Python package, followed by manual curation with the Phy program (Rossant et al., 2016). The following stringent criteria were used to ensure that only well isolated and stable neurons would be analyzed: (1) discriminable action potentials of no less than a 3:1 signal-to-noise ratio; (2) continuous activity across the entire experiment; and (3) clear refractory period of 1 ms in the autocorrelation function. Since this study was designed to investigate neuronal changes over time, deviations in neuronal basal or response activity were not considered excluding criteria, unlike in shorter recording protocols.

Perfusion

At the end of the experiment, the rats were anesthetized with KX solution and then perfused with saline (0.9% NaCl) followed by 4% formaldehyde solution. After fixation, the brain was extracted from the skull and left for 72 h in a 30% sucrose formaldehyde solution at 4°C.

Histology

The fixed brains were cut into 50 µm slices using a microtome (Thermo Fisher Scientific), plated on microscope slides, covered with DAPI-containing preservative (Fluoromount-G with DAPI, Thermo Fisher Scientific), and left to dry for 24 h. Localization of the electrode bundle was accessed using a light binocular. Only rats with correct electrode localization within the GC were included in the study.

Movement analysis

Full HD (1080p) video recordings were made at 30 frames/s throughout the entire experimental period using a camera (model C920, Logitech). At the end of the experiment, the videos were analyzed using the Python Open-CV module. The movements of the rats over time were calculated by comparing the differences (in pixels) between adjacent frames of the video. The movements were then averaged over each second (30 frames) and over hours to compare between groups.

Single-neuron response analysis

To investigate whether GC neurons responded to Sac administration, we compared averaged (across 3 s) evoked firing rates to baseline (BL) firing (>1 s just before Sac administration) using paired *t* tests. A neuron for which the *t* test found significantly different ($p < 0.01$) firing rates of BL and response on the taste trials of a given phase was deemed "taste responsive" for that phase. This definition was used to calculate the percentages of taste-responsive neurons in a phase and to generate the pixel map of taste responsivity (Piette et al., 2012; Sadacca et al., 2012).

To examine changes in the single GC taste responses across the experimental phases, we divided the spiking activity of each neuron in the 2.5 s after a tasting event into consecutive 50 ms bins. The trials were aggregated into experimental time phases of pre-CTA, and 1, 2, 3, 3–6, 6–12, and 12–18 h post-CTA, and were normalized by dividing the results by the mean BL activity in the 1 s before the aggregated responses. To identify neurons that changed after consolidation, we compared the normalized pre-CTA and 12–18 h taste responses using a two-way ANOVA with session (pre-CTA and 12–18 h) and response bins (50 ms bins between 0 and 2500 ms after taste stimulation) as the main factors. Significant ($p < 0.01$) session or interaction effects were termed "changed,"

otherwise the neuron was classified as "unchanged." Changes in neuronal responses across experiment times were similarly performed separately for the early epoch (EE; 200–800 ms after taste delivery) and late epoch (LE; 1000–2500 ms after taste delivery) response times.

Assessment of spike train variability

The Fano factor (FF) is regularly used to assess the variability of spike trains. Spike trains were first binned into windows of 1 s, and the spikes in each bin were counted. The FF for every minute of recording during the post-CTA time was calculated by dividing the variance of these counts by their mean in nonoverlapping windows of 60 s.

Burst analysis

A burst was defined as at least three consecutive spikes with an interspike interval of $<$15 ms. Bursts were identified and counted in the 3 s before ("BL bursts") and after ("response bursts") each tasting event. A burst ratio was calculated by dividing the response burst counts by the BL burst counts, which thus characterized the normalized change in bursting activity.

Ensemble response distance, the "normalized population response distance" metric

To assess the changes in the population representation over time, we first needed to define the pre-CTA state for the BL, EE, and LE epochs. To that end, we calculated a reference vector $\vec{v}_{\text{ref}}$ for the BL ($\vec{v}_{\text{ref},BL}$), and one for each of the epochs ($\vec{v}_{\text{ref},EE}$and$\vec{v}_{\text{ref},LE}$ for the EE and LE, respectively). Each scalar value in these N-dimensional arrays was the mean epochal FR over the 30 pre-CTA IOC tasting events of a certain neuron. To assess the population changes over time, for each experimental phase t (1 h, 2 h, ...) and epoch e (BL, EE, and LE), we calculated the vector $\vec{u}_{t,e}$ in a manner similar to $\vec{v}_{\text{ref}}$ but using all the taste trials of phase t and the FR in epoch e. Next, we calculated the "norm distance" $D_{e,t}$ between the two vectors to assess the distance of the current population representation of the epoch from its pre-CTA representation, as follows:

$$D_{t,e}(\vec{u}_{t,e}, \vec{v}_{\text{ref},e}) = \frac{\|\vec{u}_{t,e} - \vec{v}_{\text{ref},e}\|}{\|\vec{u}_{t,e}\| + \|\vec{v}_{\text{ref},e}\|}, \quad (1)$$

where e is one of the three epochs, t is a block of taste trials, and $\| \bullet \|$ denotes the Euclidean norm of the vector. To account for possible drift and BL changes, we further normalized the norm distance by performing element-wise subtraction of the BL distance series from the EE and LE series to form the "normalized population response distance" (NPRD) metric, as follows:

$$\text{NPRD}_{t,e}(\vec{u}_{t,e}) = D_{t,e} - D_{t,BL}, \quad (2)$$

where notations are as defined above, and e is either EE or LE. We thus obtained two series of numbers (NPRD for EE and LE) representing the distances from the mean pre-CTA vector spanning the experimental phases. Similarly, the $D_{t,BL}$ was used to represent the deviation of the population BL activity from its pre-CTA state.

Assessing the pattern of LE taste response increases and decreases in the population over time

To probe the relationship between LE increases and decreases in the population over time, we first calculated the mean and SD of the LE responses (1000–2500 ms post-taste delivery) for each neuron during the pre-CTA phase. Next, the firing rate in the LE of each trial during the post-CTA time was normalized to a z score by subtracting the mean and dividing by the SD of the pre-CTA phase. These values were then averaged for each neuron in each experimental phase. To visualize the results of these calculations (separately for the Fam and Exp groups), we represented them as heatmaps (see Fig. 6*D*). A large negative value indicates a strong decrease compared with pre-CTA, and a large positive value indicates a strong increase. To evaluate the relationship between increases and decreases in the population over time, we calculated the Pearson correlation between the percentage of neurons with a z score >1 and those with a z score less than -1 (see Fig. 6*D*, colored lines).

Ensemble-state dynamics analysis

We assessed the timing of the underlying states in GS ensembles using a Poissonian hidden Markov model (HMM; Rabiner, 1989; Kemere et al., 2008; Ponce-Alvarez et al., 2012; Moran and Katz, 2014). Our model was constructed from three consecutive feedforward states: one for the BL, and two more for the early and late response states. Trials were grouped into the following five experimental phases: pre-CTA, 0–3 h (CTA acquisition), 3–6 h (Intermediate), 6–12 h (Consolidation), and 12–18 h. HMM training was performed separately for each recorded session and spiking activity of trials from a specific experimental phase. Spike trains were first compiled into 10 ms bins to produce momentary spike rate sequences. The probability of maintaining the same state was randomly initialized to values between 0.95 and 0.99 for the BL and EE states, and 1 for the late state. Accordingly, the initial probability of transitioning to the next state in the sequence was 1-P(maintain state) for all states. Firing rates for the BL, early state, and late state were initialized to the mean spontaneous rate in the 3 s preceding a taste delivery (BL), the mean firing rate during the first 200–800 ms of poststimulus time (EE), and the mean firing rate during the 1000–2500 ms poststimulus time (LE), respectively. Training of the HMM was performed by application of the forward–backward algorithm; the EM procedure incrementally refined the firing rate and the state transition matrix parameters. We repeated this HMM training procedure 200 times while adding random changes to the initial conditions, and eventually using the final state transitions and firing rate matrices with the highest likelihood. We then used the trained model to calculate the posterior probability of the ensemble being in each of the states at each point in time for each trial. At each time bin, the ensemble was considered to be in the state that had the highest probability.

Long short-term memory classifier

A long short-term memory (LSTM) classifier model (Sherstinsky, 2020) was created using the Keras and TensorFlow packages to reveal the progression of changes in the population (see Fig. 7*D*). The LSTM classifier was implemented since it uses sequential data as input (and therefore is sensitive to the dynamics of the population response) but is insensitive to minor changes in the sequence (FR changes in only some of the neurons). Specifically, the LSTM binary classifier was trained on the pre-CTA and 12–18 h post-CTA neuronal response trials, and was later used to classify the intermediate phases. The model architecture had an input layer with 32 LSTM nodes, which received an input matrix with a shape of $60 \times N$ where 60 was the number of 50 ms bins in a 3 s response, and N was the number of neurons. This layer had a 15% dropout and a 15% recurrent dropout (i.e., 15% of nodes were randomly deleted in each training epoch), which was used to facilitate the acquisition of more general features. The LSTM layer was followed by two dense hidden layers with 32 and 16 nodes, respectively, using a ReLU activation function, after which we added batch normalization for faster training and a 15% dropout between the layers. The model output layer had two nodes with a softmax activation function. The model was trained on a randomly selected set of 70% pre-CTA and 12–18 h post-CTA trials, with 15 random model initializations, and was tested on the remaining 30% of the trials. The model was optimized using the rmsprop optimizer with "binary cross entropy" and "accuracy" as the loss and metric. Once the model was trained, it was used to predict the probability of each trial from all experimental times to be classified as either pre-CTA or 12–18 h.

Statistical analysis

All multicomparison statistical analyses were performed using either a one-way or two-way ANOVA with a *post hoc* analysis using two-tailed Student's t tests. Differences in the percentage of neurons between the groups across time were tested using the χ^2 test. All error bars in the graphs express the SEM. The significance level was set at $p < 0.05$ for all tests unless otherwise specified.

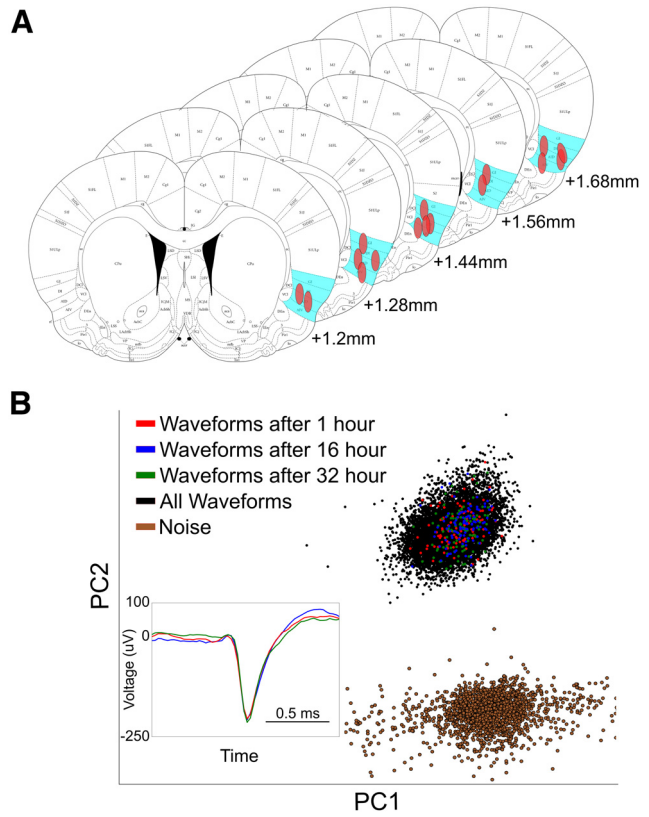

Figure 2. Data validation. ***A***, Localization of the electrode bundle (red ovals) within the GC (shaded cyan area) of rats included in the analyses, projected on the illustrated coronal sections. ***B***, The shape of all spikes of an example neuron collected across the entire experiment projected on a 2D space following PCA. Colored dots indicate waveforms from 3 different hours (1, 16, and 32 h) of the recording session. Inset shows the mean waveforms collected during these hours. The spike projections are well clustered and far from the noise cluster (brown dots); a good indication of a well isolated unit. The high similarity between the waveforms across hours is indicative of the high stability of the neuronal recording throughout the experiment.

Data availability
Data will be made available on reasonable request.

Results

The custom-built cage and electro-fluid commutator (Fig. 1*B*) allowed the rats to move freely and sleep with minimal interruptions during the 8 d protocol (Fig. 1*A*). GC neuronal activity from the Exp ($n = 7$: males = 5, females = 2) and Fam ($n = 7$: males = 4, females = 3) rat groups were recorded continuously for 2 consecutive days (from 24 h before until 24 h after CTA training). Postexperiment electrode position assessment ensured correct localization of the electrode wires within the GC (Fig. 2*A*). The recorded extracellular signals were processed offline to extract and sort neuronal spiking activity. Stringent criteria were used to ensure that only units clearly isolated from the background noise across the entire recording time (Fig. 2*B*) and that maintained similar waveform (Fig. 2*B*, inset) were included in the experimental cohort (see Materials and Methods).

Naive rats learn CTA but not when familiarized with the conditioned taste

On the CTA training day (day 7; Fig. 1*A*), animals in the Exp and Fam groups drank similar amounts of Sac solution from the two bottles (Fig. 3*A*; *t* test: $t = 0.251$, $p = 0.803$). The level of CTA learning was tested with a two-bottle test on the morning of the next day. As expected, the Exp group showed significantly higher aversion to Sac than the Fam group after training (Fig. 3*B*; *t* test: $t = 4.26$, $p = 0.002$), an indication of an LI effect. Because neural activity across the entire brain, even in the primary sensory cortices, is highly affected by motor activity (Musall et al., 2019; Stringer et al., 2019), we also monitored the movement of the rats using an in-cage camera but found no significant difference between the groups over the post-training hours (Fig. 3*C*; two-way ANOVA: group: $F_{(1)} = 0.16$, $p = 0.68$; group × time: $F_{(1,9)} = 1.03$, $p = 0.41$). Together, these results confirm that while both groups went through an identical CTA procedure, they differed in their CTA learning, thus setting the stage for an examination of the progression of changes in the GC neuronal activity that underlies the learning process.

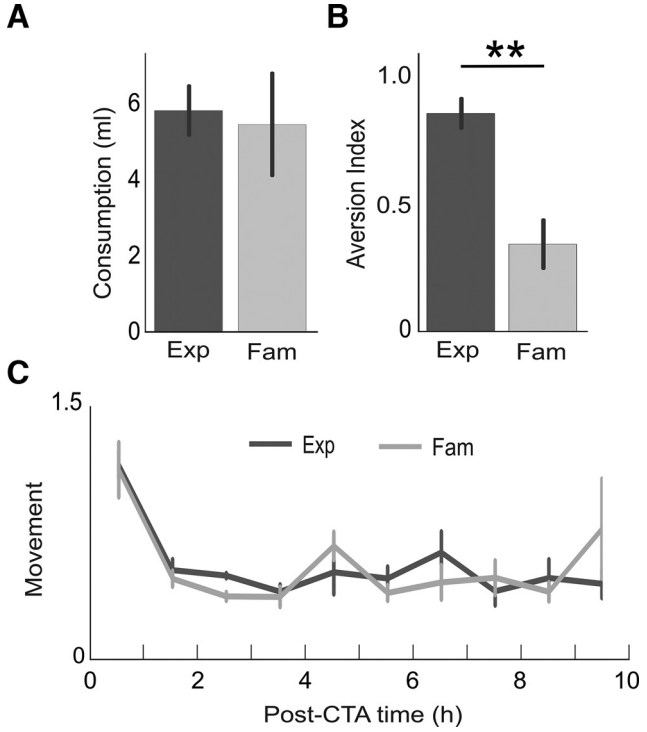

Figure 3. Behavioral results. ***A***, Saccharin consumption by the Exp and Fam rats during the training day. ***B***, Aversion index calculated after CTA on the test day. Exp rats showed a significantly higher aversion to Sac than the Fam rats. ***C***, Movement of rats over time, calculated from continuous video recordings of the experimental cage, showed no significant difference between groups. The similar increase in activity during the first hour is the outcome of postdrinking feeding activity. $**p < 0.01$.

Learning does not alter the basal neuronal activity properties of the population over time

We recorded 100 and 105 neurons from the Exp and Fam groups (mean ± SEM: Exp, 14.3 ± 3.0 neurons/animal; Fam, 15 ± 3.3 neurons/animal), of which 78 and 76 neurons, respectively, were eventually used after applying the stringent excluding criteria of stability, signal-to-noise ratio (Fig. 2*B*), and refractory period (see Materials and Methods). Unless otherwise stated, these well isolated neurons were used in the analyses below. Examples of basal activity across 10 h from four different neurons are shown in Figure 4*A*. While a minor slow drift effect could be observed in the baseline activity of some of the neurons, most neurons exhibited stable activity although jittery. Averaging over all neurons of the Exp and Fam groups showed fluctuations around a mean of ~8 spikes/s (Fig. 4*B*), with no significant difference

between groups (two-way ANOVA: group: $F_{(1)}$ = 0.61, $p = 0.43$; group × time: $F_{(1,9)} = 1.5$, $p = 0.13$). Similarly, no difference was found in the variability of the spike trains (the "regularity" of the spikes in a certain time window), as measured by the FF (Fig. 4*C*; two-way ANOVA: group: $F_{(1)} = 0.31$, $p = 0.574$; group × time: $F_{(9)} = 1.52$, $p = 0.13$). Interestingly, both groups displayed a more regular firing rate in the hour following the LiCl injection, as indicated by the lower FF values and a return to a Poissonian pattern (irregular spike sequences, with FF values near 1) thereafter (Fig. 4*C*). The early low FF values were probably related to the LiCl-induced sickness that is known to last for about an hour and was experienced by both groups. Together, the similarity in the movement and neuronal baseline activity characteristics of the two groups provided a solid starting point for studying the temporal evolution of learning-related taste response changes.

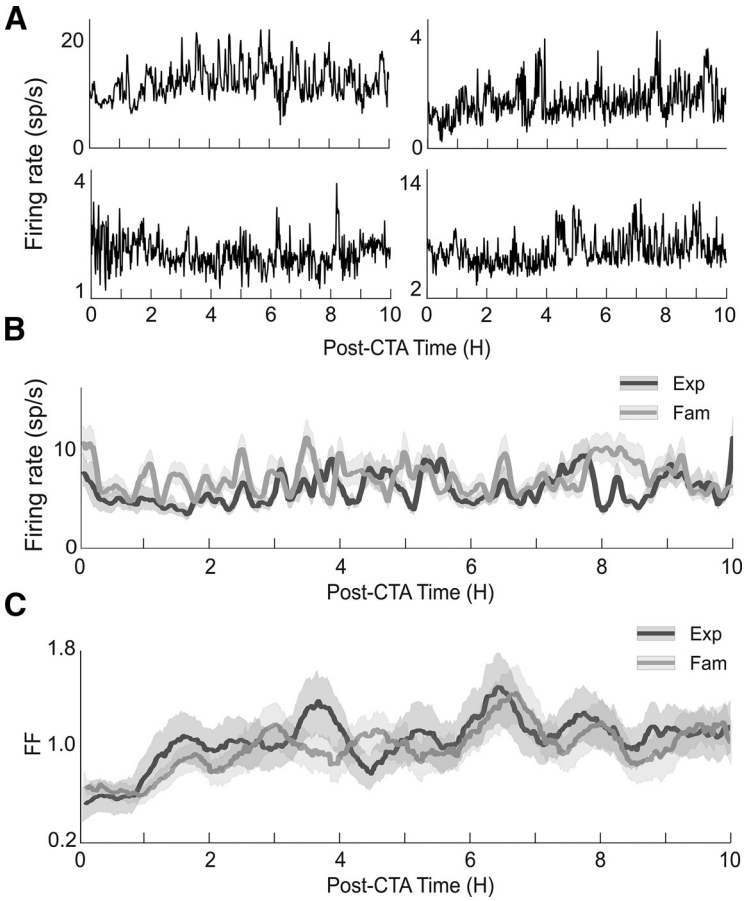

Figure 4. Similar basal neuronal firing rate characteristics between the groups. ***A***, Example firing rates over time in 1 min bins of different neurons from both the Exp (left) and Fam (right) rats. ***B***, Averaged FR of all neurons in both groups over the 10 h following CTA training. ***C***, Averaged Fano factor of all neurons in both groups over 10 h following the LiCl injection. Data are represented as the mean ± SEM. Sp/s, Spikes per second.

Taste response changes of single GC neurons to the conditioned taste following CTA

When tested 18 h after CTA induction, some of the GC neurons showed altered responses to the Sac (Fig. 5*A*, top), whereas others remained unchanged (Fig. 5*A*, bottom), which is consistent with previous reports (Moran and Katz, 2014). These response changes were likely related to learning. For instance, the number of neurons that were found after 18 h with a response that differed from the one observed during pre-CTA was three times higher in the Exp group than in the Fam group [Exp, 23.1% (18 of 78); Fam, 7.9% (6 of 76); χ^2 test: $\chi_{(152)} = 6.34$, $p = 0.0012$). Additionally, the mean response magnitude to Sac across all neurons during the first 3 s increased significantly after 18 h in the Exp group, but not in the Fam group (Fig. 5*B*, left; *t* test; Exp: $t_{(152)} = 2.85$, $p = 0.006$; Fam: $t_{(152)} = 1.345$, $p = 0.181$), or in the responses to water in both groups (Fig. 5*B*, right; two-way ANOVA: group: $F_{(1)} = 0.97$, $p = 0.32$; time: $F_{(1)} = 0.31$, $p = 0.58$; group × time: $F_{(1,1)} = 0.87$, $p = 0.35$). Recording continuously over the hours following CTA induction allowed for scheduled inspection of the progression of neuronal response changes. Based on previous studies, we partitioned the post-CTA time into several phases, as follows: 0–3 h (CTA acquisition), 3–6 h (intermediate phase), 6–12 h (consolidation), and 12–18 h (postconsolidation). Figure 5*C* shows examples of four neurons and their progression of response changes over time. While the response of the neuron in Figure 5*Ci* remained stable over the post-CTA time, the other three examples show a diverse pattern of changes, both in the time when changes occurred and in the direction of changes (increased or decreased). We conducted several analyses to characterize the progression of changes at the single-neuron level following CTA induction. To achieve a better resolution of the changes during the acquisition phase, in which the malaise occurred in both groups but CTA acquisition developed only in the Exp group, we partitioned the 0–3 h phases into three hourly phases (1, 2, and 3 h). We found that CTA increased the number of taste-responsive neurons in the Exp group during the acquisition (2 h) and following the consolidation phase (6–18 h; Fig. 5*D*; χ^2 test: 2 h: $\chi_{(152)} = 11.64$, $p < 0.001$; 6–12 h: $\chi_{(152)} = 6.48$, $p = 0.011$; 12–18 h: $\chi_{(152)} = 5.58$, $p = 0.018$).

The fluctuation in the number of taste-responsive neurons over time may be the outcome of the same neurons becoming responsive and then unresponsive, or of more complex transitions within the population. To compare these two alternatives, we created pixel maps in which each row depicts the responsiveness (true/false) of a certain neuron in the different post-CTA phases (Fig. 5*E*). The neurons in the pixel map were ordered according to their pre-CTA state (Fig. 5*E*, bottom, responsive neurons; Fig. 5*E*, top, unresponsive neurons, delineated by a red line), and similarly for the other phases (those responsive in the 1 h, 2 h, etc.). The pixel maps, generated separately for the Exp (Fig. 5*E*, left) and Fam (Fig. 5*E*, right) groups, showed a plethora of responsiveness dynamics over the experimental phases. When we calculated the percentages of responsive neurons separately for neurons that were taste-responsive during pre-CTA (Fig. 5*F*, bottom) and those that were not (Fig. 5*F*, top), we found that the early increase in responsive neurons during CTA acquisition (at 2 h) originated from both pre-CTA responsive and unresponsive neurons (*t* test Exp vs Fam: responsive at pre-CTA: 2 h, $p < 0.001$; unresponsive at pre-CTA: 2 h, $p < 0.001$). In contrast, the increase in responsive neurons during the consolidation phase originated solely from recruiting neurons that were unresponsive during pre-CTA (*t* test Exp vs Fam: 3–6 h, $p = 0.023$; 6–12 h, $p = 0.011$). Overall, responsivity to the conditioned taste in the single-neuron level thus appeared to be a highly dynamic property.

A neuron may be taste responsive during the pre-CTA and post-CTA phases, but these responses may differ in their magnitude

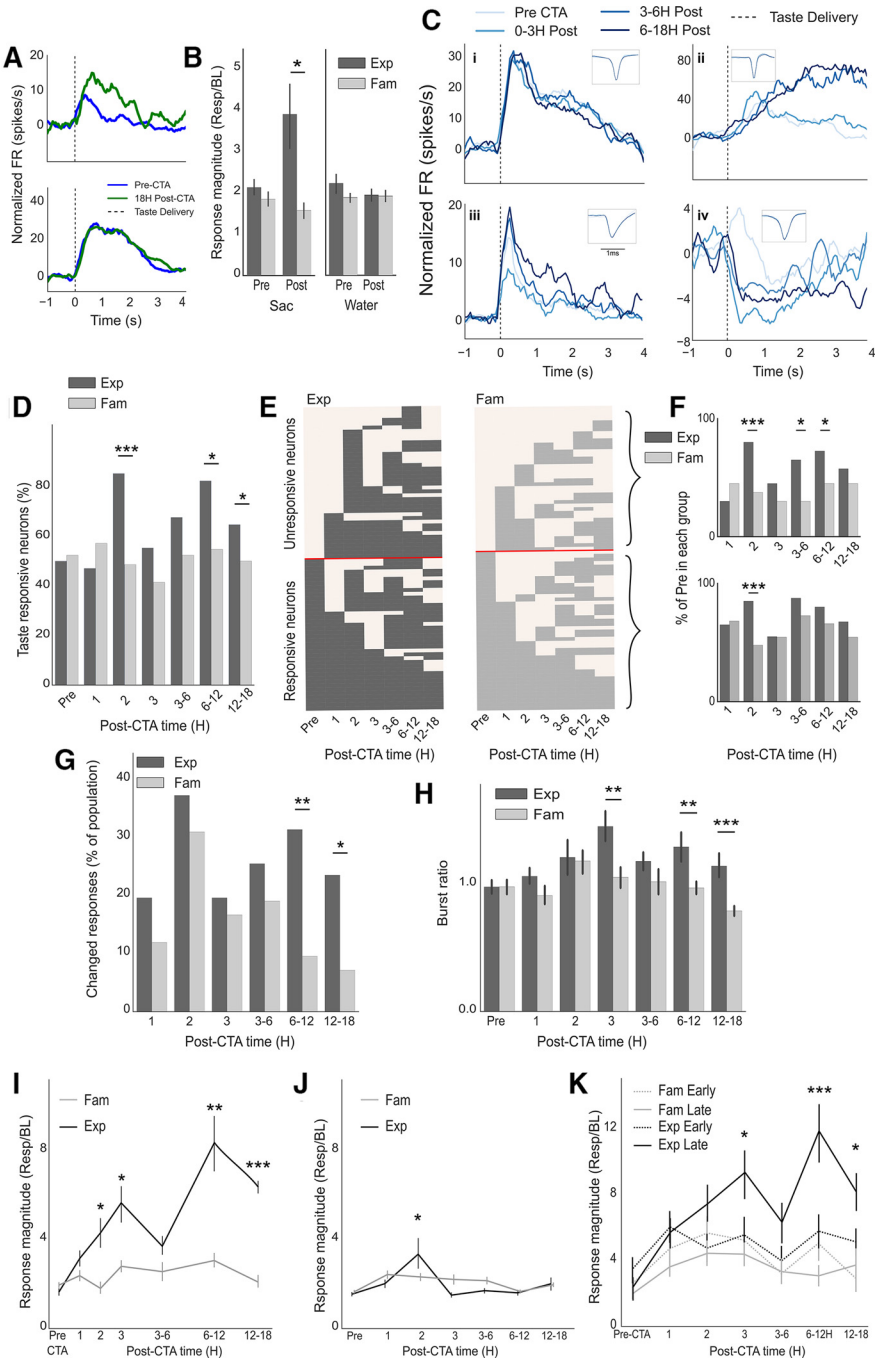

Figure 5. Post-CTA changes in the responses of GC single neurons. ***A***, Example of two neurons, one that changed its mean response to Sac 18 h after CTA learning (top) and another that did not (bottom). The graphs represent the mean response of the neurons to Sac stimulation normalized to their baseline activity. ***B***, Averaged Sac response magnitude over all neurons 18 h post-CTA. Sac response magnitude increased in the Exp rats but not in the Fam rats (left), but remained unchanged for water in both groups. ***C***, Example neurons that changed their response to Sac in different phases following CTA training. ***D***, Percentage of Sac responsive neurons over the 18 h post-CTA training. Exp, $n = 78$; Fam, $n = 76$. ***E***, A pixel map representing the Sac responsiveness of each neuron (lines) across the experimental phases (columns). Gray and beige fills indicate Sac responsiveness and unresponsiveness, respectively. Neurons were ordered according to their responsiveness over the phases. Red horizontal lines differentiate responsive from unresponsive neurons during the pre-CTA phase. ***F***, Percentage of Sac-responsive neurons over the 18 h post-CTA training, divided into neurons that were Sac responsive before CTA (bottom), and those that were not (top). Whereas the higher number of Sac-responsive neurons during the early CTA acquisition originated from both pre-CTA responsive and unresponsive neurons (at 2 h), the increase in the consolidation phase relied on the recruitment of pre-CTA unresponsive neurons. ***G***, The percentage of neurons that changed their response to the conditioned taste from the pre-CTA response. Exp, $n = 78$; Fam, $n = 76$. ***H***, Normalized bursting activity during Sac responses over post-CTA hours. ***I***, Averaged response amplitude over the time of neurons that had significantly different Sac responses 18 h post-CTA compared with pre-CTA (Exp, $n = 18$; Fam, $n = 6$). ***J***, Population response amplitude over time of neurons that had similar Sac responses between pre-CTA and 18 h post-CTA (Exp, $n = 60$; Fam, $n = 70$). ***K***, Similar analysis as in ***I***, conducted separately for the EE (200–800 ms) and LE (1000–2500 ms) over post-CTA hours shows that changes in the LE amplitude dominated the changes during the acquisition and consolidation phases. $^{*}p < 0.05$, $^{**}p < 0.01$, $^{***}p < 0.001$.

and structure. To track these fine-grained changes, we calculated the percentage of neurons whose taste response deviated from their pre-CTA response. We found that the percentage of these neurons increased 2 h post-CTA, followed by a decline an hour later in both groups (Fig. 5*G*). However, while these percentages continued to decline in the Fam group during and after the consolidation epoch, they were significantly higher in the Exp group (Fig. 5*G*; χ^2 test: 6–12 h: $\chi_{(152)} = 7.31$, $p = 0.006$); 12–18 h: $\chi_{(152)} = 6.34$, $p = 0.012$). Similar significant increases during the acquisition and consolidation phases were found in neuronal bursting activity, which is known to be associated with learning (Mason and Rose, 1988; Laviolette et al., 2005; Li et al., 2007; Fig. 5*H*; two-way ANOVA: group: $F_{(1)} = 16.527$, $p = 0.0006$; time: $F_{(6)} = 3.8$, $p = 0.001$; group × time: $F_{(1,6)} = 1.66$, $p = 0.13$; *t* test: 3 h: $t_{(152)} = 2.82$, $p = 0.006$; 6–12 h: $t_{(152)} = 2.94$, $p = 0.0048$; 12–18 h: $t_{(152)} = 4.19$, $p = 0.0001$).

We considered the neurons that maintained a different response after 18 h than the pre-CTA (postconsolidation) as part of the CTA memory engram (Poo et al., 2016). We specifically followed these neurons back to the pre-CTA time to identify the dynamic nature of their response amplitude changes over the post-CTA time. We found that while neurons in the Fam group ($n = 6$) showed on average a low and constant response magnitude over time, the average of the response of neurons in the Exp group ($n = 18$) showed a double-peak increase: one weaker peak during CTA acquisition and another stronger one during and after consolidation (Fig. 5*I*; two-way ANOVA: group: $F_{(1)} = 25.375$, $p = 10^{-6}$; group × time: $F_{(1,6)} = 3.04$, $p = 0.007$; *t* test: 2 h: $t_{(22)} = 2.87$, $p = 0.011$; 3 h: $t_{(22)} = 2.45$, $p = 0.021$; 6–12 h: $t_{(22)} = 2.922$, $p = 0.007$; 12–18 h: $t_{(22)} = 8.52$, $p < 10^{-8}$). Interestingly, neurons in the Exp group ($n = 60$) that had a similar taste response on the pre-CTA and 18 h post-CTA still showed a weak but significant response increase 2 h post-CTA (Fig. 5*J*; two-way ANOVA: group: $F_{(1)} = 0.53$, $p = 0.468$; group × time: $F_{(1,6)} = 2.77$, $p = 0.011$; *t* test: 2 h: $t_{(128)} = 2.44$, $p = 0.016$). This suggests that neurons that were in the early, acquisition-related part of the learning, could have ended up out of the final CTA memory engram. Finally, GC neurons are known to sequentially code taste identity and palatability (the hedonic value of a taste): an early identity coding epoch (EE, 200–800 ms) is followed by a late palatability coding epoch (LE, 1000–2500 ms). Since CTA alters the hedonic value of a taste, we expected that the progression of response magnitude changes depicted in Figure 5*I* would primarily be the result of changes in the LE. This is indeed what we found when we measured magnitude changes separately for the EE and LE over time. The double-peak change pattern was visible in the LE (Fig. 5*K*; *t* test: Exp EE vs LE: 3 h, $p = 0.05$; 6–12 h, $p = 0.004$; 12–18 h, $p = 0.04$), whereas in the Fam and Exp-EE, the magnitude generally remained unchanged. Together, these results suggest that on the GC single-neuron level, memory-related response changes do not accumulate slowly in specific neurons, but rather occur over most of the population in various phases. Across the population, these "chaotic" changes are averaged into a more structured increased response that is locked to the CTA acquisition and consolidation phases, which are probably aimed to alter the LE palatability coding.

Population response changes start immediately after CTA induction

Inspecting changes in the communal amplitude of single neurons showed a double-peak pattern in the hours following CTA learning, but this type of averaging may mask more fine-grained changes in the population activation (e.g., balanced excitations and inhibitions that cancel each other out). Instead, here we represented the GC ensemble activity of a rat during a certain experimental phase (and separately for the BL, EE, and LE) as an N-dimensional vector, where N was the number of neurons recorded simultaneously from that rat, and where each element of the vector represents the mean FR of a neuron in the corresponding epoch (see Materials and Methods). Figure 6*A* shows example trajectories of these ensemble vectorized representations over time (Fig. 6*A*, top; LE, bottom; BL), projected on a 2D plane [using principal component analysis (PCA)] for Exp (Fig. 6*A*, left) and Fam (Fig. 6*A*, right) rats. Whereas the Exp response trajectory (Fig. 6*A*, top left) appears to deviate more robustly from the initial pre-CTA representation, the Fam shows an unstructured, more random, progression. To quantify this observation, we calculated the NPRD (see Materials and Methods) metric that measures the difference between the population representations at a certain experimental phase and the pre-CTA phase, normalized to changes in the BL representations at these similar phases. Low values of NPRD (near 0) indicate minor changes in the population taste representation. As expected, this indeed was the case for the NRPD of the water trials (Fig. 6*B*), where no significant difference was found between groups and epochs across the experimental phases (three-way ANOVA: group × time × epoch: $F_{(1,5,1)} = 5.91$, $p = 0.31$). A similar analysis for Sac (Fig. 6*C*), however, found a significant interaction among groups, experimental phase, and epochs (three-way ANOVA: group × time × epoch: $F_{(1,5,1)} = 13.04$, $p = 1.49 \times 10^{-12}$). Further analysis revealed a significant difference between the groups in the palatability-rich LE (Fig. 5*D*; two-way ANOVA: group: $F_{(1)} = 50.29$, $p = 8.54 \times 10^{-22}$; group × time: $F_{(1,5)} = 9.33$, $p = 4.26 \times 10^{-15}$), which was higher in the Exp group compared with the Fam group over the entire post-CTA time (Fig. 6*C*; *t* tests: Exp EE vs Exp LE: 1 h, $p = 0.039$; 2 h, $p = 0.011$; 3 h, $p = 0.038$; 3–6 h, $p = 3.3 \times 10^{-12}$; 6–12 h, $p = 0.002$; 12–18 h, $p = 0.006$). Surprisingly, the population response kept changing during the 3–6 h phase (Fig. 6*C*), whereas the averaged magnitude response of single neurons showed a reduction during this time (Fig. 5*I*,*K*). These results suggest that the overall changes in magnitude might not constitute a return of single neurons to their pre-CTA responses, but rather are the result of some balancing, more general homeostatic, processes. To further study this supposition, we ordered the neurons of each experimental group at each time according to their *z*-score deviation from pre-CTA responses in the LE (Fig. 6*D*). When we compared the relationship between the percentage of neurons that increased and decreased their responses throughout the experiment (using *z* scores of ± 1), we found a clear difference between the two groups, as follows: in the Fam group increases and decreases were anticorrelated ($r = -0.71$), whereas in the Exp group they were positively correlated ($r = 0.29$). These results support the hypothesis that learning involves ongoing delicately balanced increases and decreases in the response FR of GC neurons (which do not necessarily cancel each other out). Together, these results suggest that the learning-induced amplitude increases in the LE of GC neurons may have been the result of continuous changes in the LE ensemble response representation, a progression that is characterized by structured interaction between increases and decreases of the FR in the neuronal population.

Learning-induced ensemble-state dynamics quickening only occurs following CTA consolidation

In the GC, coding of taste identity and palatability has also been reported in ensemble-state dynamics (Jones et al., 2007; Moran and Katz, 2014). Specifically, tastes elicit sequences of ensemble activity states that are taste specific and faithfully track the hedonic value of the taste such that aversive tastes (both innate and learned) are processed quicker than palatable tastes (Moran and

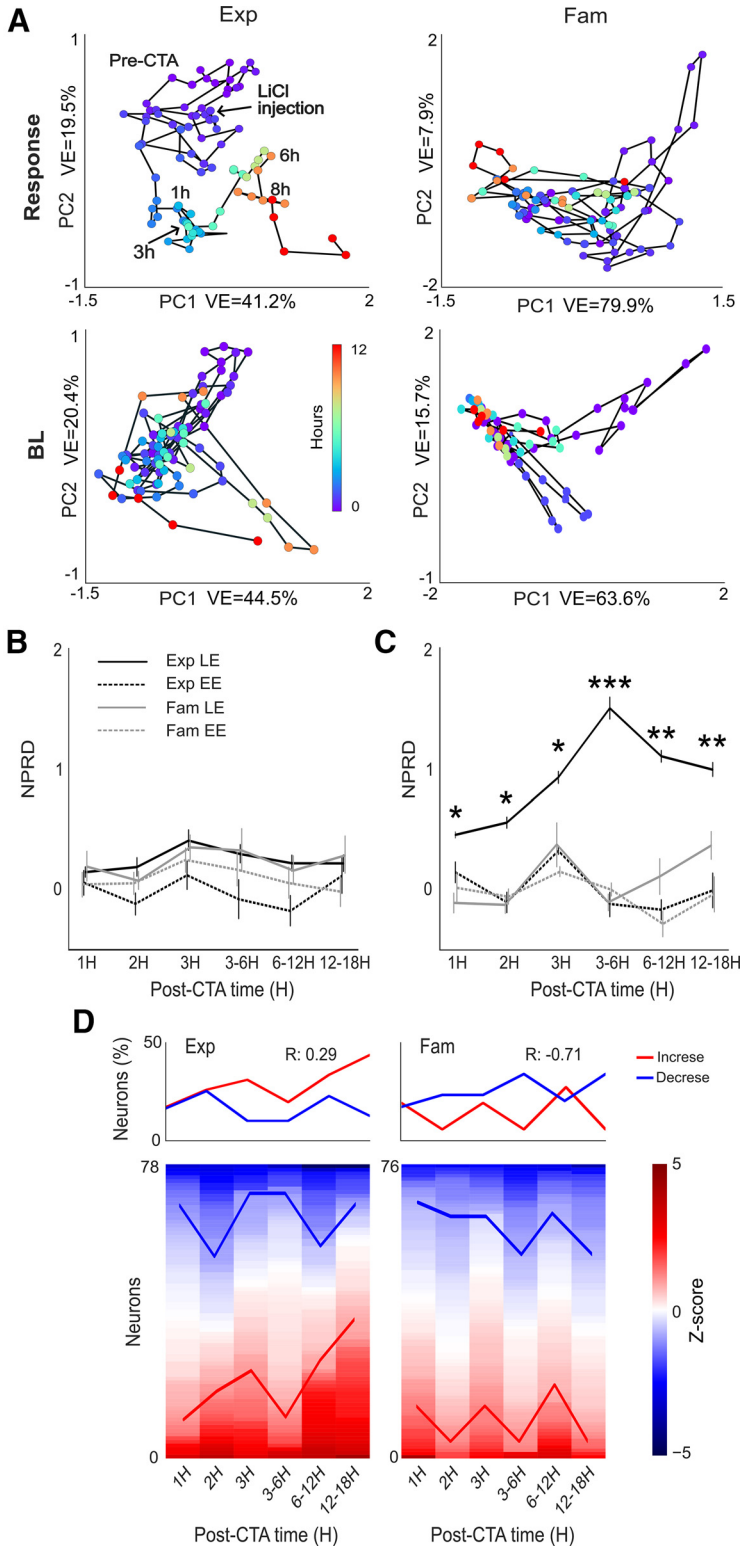

Figure 6. The LE population responses to the conditioned taste change continuously. ***A***, Example of LE ensemble Sac responses (top) and BL (bottom) over experimental times, projected on a 2D PCA space, from Exp (left) and Fam (right) rats. Each dot represents the mean ensemble response over a given batch of trials, color coded for the time from CTA induction. The percentage of variance explained ([dot]VE) by each PC is marked adjacent to each axis. Whereas in the Exp rats the Sac response of the ensemble appeared to increase its distance from the origin, in the Fam rats the changes were more local. ***B***, The average deviation from their pre-CTA state of the water EE and LE vectorized representations across time for Exp and Fam animals. There was no significant change over time between groups or epochs. ***C***, Similar to ***B*** but for Sac stimulations. The LE of the Exp rats showed an increased deviation from pre-CTA values compared with the EE of the Exp, and EE and LE of the Fam group across all post-CTA times. The change was maximal during the 3–6 h phase. Significance markers represent *t* tests comparing EE and LE in the Exp group. ***D***, Bottom, Heatmap representations of the response changes in the LE across all neurons in the Exp (left) and the Fam (right) groups. Each colored rectangle denotes the normalized difference in the LE FR between pre-CTA and a specific time during the experiment, represented as *z* scores. Neurons were ordered according to the *z*-score values at each phase. Colored lines connect the ±1 *z*-score values in each phase, indicating the percentage of neurons at ±1 *z* score. Top, The percentage of neurons that corresponds to the ±1 *z*-score lines are presented. Exp group percentages showed a positive correlation between increasing and decreasing neuronal responses, which indicates a structured change in the network, whereas neurons from the Fam group showed anticorrelation, suggesting a drift effect. $^{*}p < 0.05$, $^{**}p < 0.01$, $^{***}p < 0.001$.

Katz, 2014). The emergent time of this ensemble quickening may reveal a great deal about the role they play in CTA learning: if quicker ensemble dynamics appear as early as the single neurons, they will be linked to the behavioral response, whereas if they appear later (after 6 h), they are probably related to consolidation processes. To test this, a separate three-state HMM model (Fig. 7*A*) was trained to identify BL, EE, and LE for each ensemble and phase. Examples of four single-trial state probabilities for the same ensemble across the experiment times are shown in Figure 7*B*. These examples show that from pre-CTA until 3–6 h post-CTA, the EE-to-LE transition occurred at ~1500 ms after taste administration (Fig. 7*B*, three top panels), but earlier, at ~900 ms, in the 6–12 h post-CTA, consolidation phase (Fig. 7*B*, bottom panel). This phenomenon was evident as well when we compared the transition time across groups; namely, we found that whereas transition time remained constant across the experiment in the Fam group (Fig. 7*C*, left; one-way ANOVA: $F_{(3)} = 1.47$, $p = 0.21$), it became significantly quicker than baseline in the Exp group (Fig. 7*C*, right; one-way ANOVA: $F_{(3)} = 3.4$, $p = 0.017$), but only during the 6–12 h phase (*t* test, pre-CTA vs 6–12 h: $t = 2.12$, $p = 0.034$). Another way to study the progression of changes in the ensemble activity across the phases consists of using a classifier. In this method, a classifier (an LSTM classifier; see Materials and Methods) was trained to distinguish between pre-CTA and postconsolidation (12–18 h) ensemble responses (one classifier for each rat; Fig. 7*D*). The LSTM classifier was chosen since it is sensitive to the temporal structure of the data, and not only the values. After the classifier could faithfully identify pre-CTA and postconsolidation trials, we used this classifier to classify ensemble responses between these two time points to study the transition patterns. If changes accumulate slowly, we expected to see a steady transition between

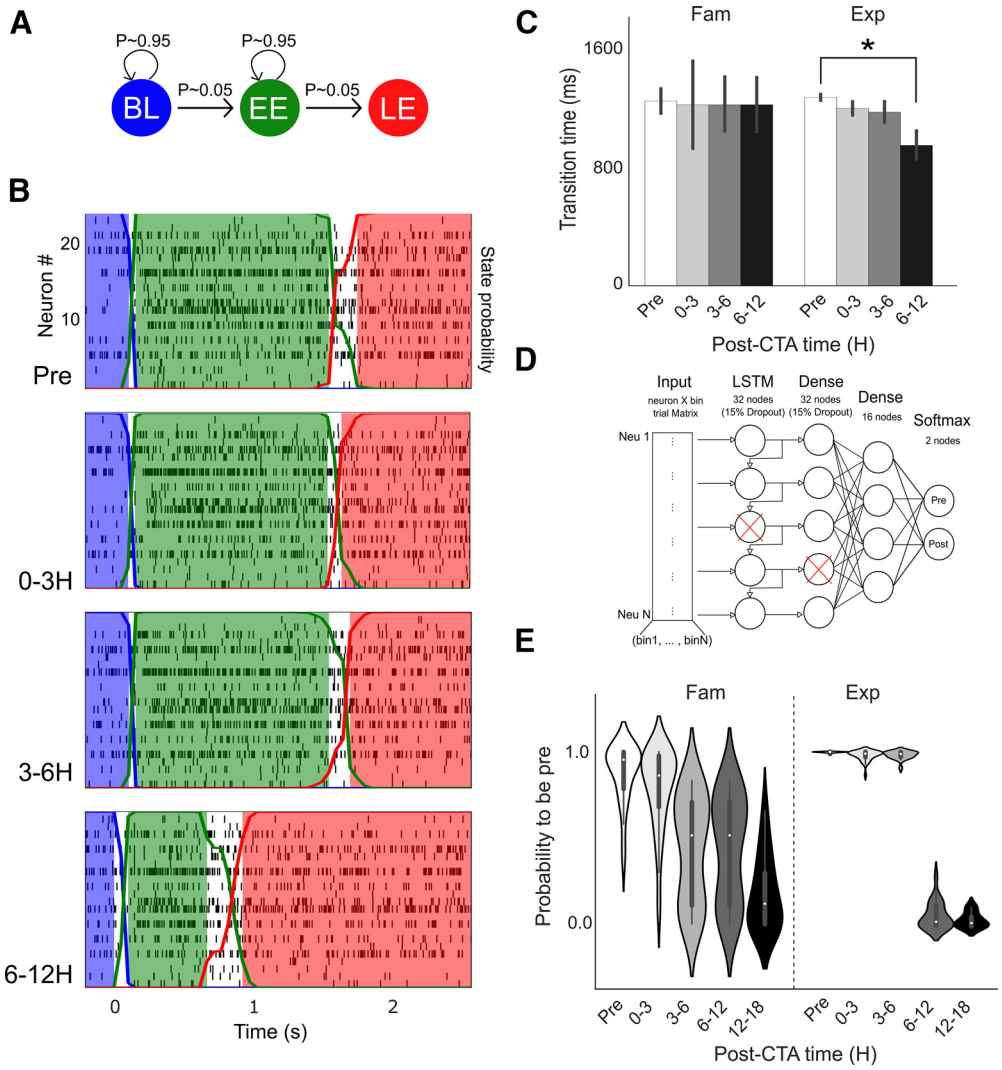

Figure 7. Ensemble dynamics shift abruptly following CTA consolidation. ***A***, The structure of the HMM model, containing the BL, EE, and LE states, as well as the probabilities (P) to transition between them. ***B***, Example ensemble responses for single Sac trials characterized using this HMM: the colored lines overlaid on the ensemble spike trains (each row is a neuron, *y*-axis) indicate the calculated probability that the ensemble is in that particular state (color coding is as in ***A***); shaded regions represent periods during which the dominant state exceeded a probability of 0.8. While the EE-to-LE transition from pre-CTA until 6 h post-CTA occurs late (~1.5 s after taste administration, 3 top panels), during the 6–12 h consolidation period, the transition occurs earlier (bottom panel). ***C***, The EE-to-LE transition time of all Sac trials, averaged separately for each phase for the Fam (left) and the Exp (right) rats, showing the quickening of the transition in the Exp group alone that appeared only after the consolidation phase (6–12 h). ***D***, Architecture of the LSTM network used to classify ensemble responses as either pre-CTA (Pre) or post-CTA. Red X denotes the 15% dropouts used for increasing the generality of classification. ***E***, Probability of a Sac trial to be classified by the LSTM network as either a pre-CTA or post-CTA trial for trials from different experimental times. While trials from Fam rats show a slow transition between classifications, Exp rats show a clear and abrupt switch 6 h after CTA learning. $*p < 0.05$.

the start and end times; otherwise, a sudden jump was expected. The results of the Fam group showed the former pattern in that the probability of being classified as "Pre-CTA" tended to decrease continuously with time (Fig. 7*E*, left). The classification results of the Exp group, on the other hand, showed a fast, step-like, transition 6 h post-training (Fig. 7*E*, right). Together, these results suggest that the neuronal FR changes that occurred throughout the post-training period, at both the single-neuron (Fig. 5*I*) and population (Fig. 6*C*) levels, were only transformed into changes in the ensemble dynamics late in the learning process, probably as the result of a consolidation-related network reorganization.

Discussion

CTA progresses through distinct memory phases of early acquisition and consolidation in the hours following training (Ferreira et al., 2002; Moguel-González et al., 2008; Ma et al., 2011; Martínez-Moreno et al., 2011), yet, the impact of these molecularly defined phases over neuronal activity remains elusive. Here we directly evaluated neuronal response changes to the conditioned tastant during the first 24 post-training hours and found that the progression dynamics of these changes differed depending on the neuronal organizational level, which can be summarized as follows: (1) single neurons changed their responsiveness to the conditioned taste in no apparent order (Fig. 5*C*,*E*); (2) population averaging over single-neuron activity characteristics such as taste responsivity (Fig. 5*D*), burstiness (Fig. 5*H*), and LE response amplitude (Fig. 5*K*) increased specifically during the early CTA acquisition and late consolidation phases, but returned to pre-CTA values during the 3–6 h, intermediate, phase; (3) vectorized representations of the responses of the ensemble deviated continuously from their pre-CTA representation

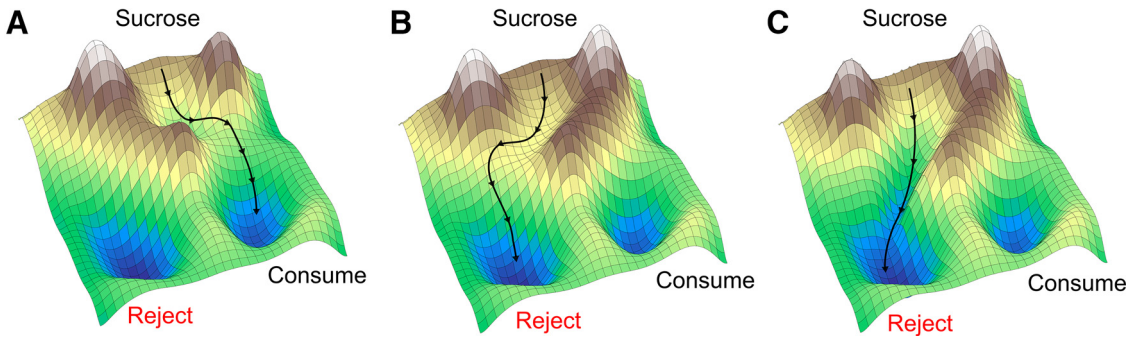

Figure 8. Landscape representation of the neuronal network across learning. The neuronal population activity can be visualized as a landscape whose features are constrained by the neuronal connectivity, and where the meta-stable states of the network appear as local dips in the terrain. The response of neurons to a taste stimulation can be modeled as a trajectory in the landscape (black line). ***A***, Before learning that the network is configured such that sucrose stimulation drives the network from the sucrose state to the "consume" decision state. ***B***, Soon after training, the network configuration changes to divert activity from the sucrose state to the reject state. ***C***, Following consolidation, the network is still configured to push the activity to the reject state, but to process sucrose faster to quickly reject it on detection.

(Fig. 6*C*), peaking during the intermediate phase; and (4) at the state dynamics level of the ensemble, the previously reported quickening of LE (Moran and Katz, 2014) appears only after the CTA consolidation phase (Fig. 7*C*,*E*). Together, these four distinct temporal progressions of changes found at the different levels of GC activity represent the complex and temporal-specific interactions that the neurons, and the network they reside within, undergo to support learning.

The main challenge of this study was to combine the different lines of results into a coherent picture of the changes that underlie memory formation. Previously, we showed a clear distinction between GC single neurons and neuronal ensemble activity changes 24 h following CTA learning: ensemble dynamics showed high fidelity with behavior, but single-neuron response changes did not (Moran and Katz, 2014). Here we were surprised to find that the neurons changed their responsivity to the conditioned taste so dynamically throughout the hours after CTA induction (Fig. 5*E*). A similar progression of neuronal representation was previously reported over longer periods (weeks) in the absence of learning (Ziv et al., 2013), but in our case, learning seemed to increase the rate of neuronal response changes considerably. Surprisingly, the rapid, seemingly unstructured, changes in the single-neuron level were balanced such that the response amplitude of the population only increased during early acquisition and after consolidation, but returned to its pre-CTA value during the intermediate phase (Fig. 5*I*). This increased response was found to relate directly to CTA learning since it was primarily driven by an increase during the palatability-coding LE (Fig. 5*K*), which is known to change after CTA (Moran and Katz, 2014) and drive typical orofacial rejection movements (Mukherjee et al., 2019). The vectorized representation of the ensemble was used to assess the level of changes in the population response without averaging; any change in the response of a neuron would deviate the vector representation from its pre-CTA representation. This analysis revealed a continuous deviation from the pre-CTA representation in the LE of the Exp group that started immediately after CTA induction. This deviation peaked during the intermediate phase (Fig. 6*C*), the same phase in which the mean response over the population returned to its pre-CTA levels (Fig. 5*I*). To possibly integrate these three lines of results, we suggest that although GC neurons continued to change their responses throughout the learning phases, a putative balancing mechanism, which is aimed to shift the palatability coding of the LE state, may govern their direction of change and excitability. Interestingly, it was recently shown that synaptic scaling, a form of homeostatic plasticity, occurs at the same intermediate phase, and is essential for the transition from general to specific CTA (Wu et al., 2021). Our current data also hint at a continuous balancing process during CTA progression in that there was a positive correlation between the number of neurons that increased or decreased their activity over the post-CTA hours (Fig. 6*D*).

Our experimental design included the Fam control group, which was pre-exposed to the Sac to attenuate CTA formation through an LI effect (Lubow, 1973, 2009). According to the current theory of LI, this pre-exposure to the conditioned stimulus (CS) without negative consequences creates a CS–"no consequence" associative memory (termed CS-0 or CS-safeness association; Lubow, 2009) that opposes the formation of CTA, thus presumably leaving learning as the primary factor for any observed difference between groups. It is possible, however, that the differences in the initial Sac exposure might themselves have induced changes that were unrelated to the CTA. For instance, exposing the Exp group to the novel taste during the tasting already initiates early taste encoding and safe learning, and the attenuation of neophobia (the reluctance to consume novel tastes; Bermudez-Rattoni, 2014; Monk et al., 2014), which do not occur in the Fam group. Furthermore, repeated exposures to the Sac during the experiment may have induced extinction in the Fam group. Therefore, the differences between the groups might not only reflect the formation of the CTA in the Exp, and the lack of it in the Fam groups, but also a more complex interaction between the above-mentioned processes and CTA. Although it is conceivable that such processes may have occurred, we believe that they had little impact on our results and conclusions. The main support for this argument comes from the striking resemblance between the current late consolidation results and our previous study (Moran and Katz, 2014) that used standard CTA protocol with non-CTA as control. At the behavioral level, the current post-CTA test of the Exp and Fam groups showed high similarity to those of Moran and Katz (2014), suggesting minor extinction effects in the Exp group and high resistance of the Fam group to the CTA. Even more astonishing were the similarities at the single-neuron and ensemble-state dynamics levels that showed the same basic results across the studies: chaotic changes in the single-neuron level, which leads to quicker transition in the state sequences. In addition, the lack of evidence for behavioral and neuronal differences between the groups during the early 2 h after Sac drinking (including similar Sac consumption in the training session) suggests low neophobia and impact

of the early taste memory process over the experiment, thus lending additional weight to our claim that the main effect that governed the differences between the groups was the formation of the CTA memory, with only negligible additional effects.

In the past few years it has become increasingly clear that the simultaneous dynamic activity of neuronal ensembles plays a vital role in brain functions (Abeles et al., 1995; Jones et al., 2007; Balaguer-Ballester et al., 2011; Okun et al., 2015). In the taste system, coherent transitions between ensemble activity states have been found to underlie innate taste-related behaviors (Jones et al., 2007; Miller and Katz, 2010; Jezzini et al., 2013; Mukherjee et al., 2019), but also to change following learning; 24 h after CTA, the ensemble-state dynamics become faster (Moran and Katz, 2014), presumably allowing for earlier detection and rejection of harmful tastes. Here we showed that this phenomenon does not emerge until 6 h after learning (Fig. 7*C*,*E*), after the consolidation phase. It is important to note that the rats displayed an aversive reaction to the taste-CS as early as 10–20 min after LiCl injection (Parker et al., 1984; Spector et al., 1988). Therefore, the faster ensemble dynamics were probably not related to the aversion memory itself, or its associated motor actions, but rather to a new rearrangement of the connectivity of the network and neuronal excitability. Our data suggest that in the GC, the role of the CTA consolidation phase is to adjust the parameters of the network (neuronal excitability and connectivity) so that the state dynamics of the ensemble become quicker. While previous studies have reported a distinction between changes at the single-neuron level and the ensemble following learning (Grewe et al., 2017), these were constrained to firing rate-based coding of the unconditoned stimulus and CS. By contrast, the current study emphasizes the dynamics of the ensemble as the pinnacle of the consolidation process.

Our findings fit and extend current dynamic system theories of brain functions. These theories model neuronal population activity, including activity related to the acquisition and maintenance of associative memories, as attractor networks (Hopfield, 1982; Amit, 1989), in which the attractors—a set of meta-stable states of population activity—represent the embedded memories of the network. Graphically, the attractor network can be represented as a landscape with some local dips denoting the states of the network (Fig. 8; Rolls, 2010). Given an external stimulus (e.g., a taste), the network activity is driven to follow a certain trajectory within this landscape. Although the sequence of meta-stable states is mostly preserved, the transition times vary and depend on numerous factors including the internal state and history of the network. Previous theoretical and experimental studies have specifically depicted this "hopping" network dynamics in GC ensemble activity that was successful in explaining the observed trial-to-trial neuronal response variability (Jones et al., 2007; Miller and Katz, 2010; Moran and Katz, 2014; Mazzucato et al., 2015; Sadacca et al., 2016). Importantly, in attractor networks, different network architectures and neuronal activity patterns can produce similar network output (e.g., reaching one of several "decision" states in the state–space landscape; Fig. 8*B*,*C*). This may explain the ongoing changes in the single-neuron and ensemble activity that still drives the same rejection behavior: while the landscape of the network keeps changing, the taste will still push the network toward the "reject" state, but with a distinct trajectory and dynamics. Our results suggest that the reorganization of the attractor network during the consolidation phase aims not only to stabilize the memory but also to speed up its processing, potentially by recruiting previously unresponsive neurons (Fig. 5*F*).

Overall, our results highlight the evolution of neuronal changes at different levels of analysis subsequent to a single trial of taste–malaise-associated learning. They highlight the distinct progression of low-level (cellular response amplitudes), mesoscale (ensemble vectorized representations), and higher-level (network dynamics) changes during different phases of learning. These specific progressions of change are known to underlie complex dynamical systems, where the behavior of the system cannot be directly predicted from the behavior of its components. Nevertheless, further studies are required to elucidate the fine-grained changes in the interneuronal connectivity and internal excitability of the neurons that support the creation, stabilization, and maintenance of memories.

References

Abeles M, Bergman H, Gat I, Meilijson I, Seidemann E, Tishby N, Vaadia E (1995) Cortical activity flips among quasi-stationary states. Proc Natl Acad Sci U S A 92:8616–8620.

Aceti M, Vetere G, Novembre G, Restivo L, Ammassari-Teule M (2015) Progression of activity and structural changes in the anterior cingulate cortex during remote memory formation. Neurobiol Learn Mem 123:67–71.

Aizenman CD, Huang EJ, Manis PB, Linden DJ (2000) Use-dependent changes in synaptic strength at the Purkinje cell to deep nuclear synapse. Prog Brain Res 124:257–273.

Amit DJ (1989) Modeling brain function. Cambridge, UK: Cambridge UP.

Bailey CH, Kandel ER (1993) Structural changes accompanying memory storage. Annu Rev Physiol 55:397–426.

Balaguer-Ballester E, Lapish CC, Seamans JK, Durstewitz D (2011) Attracting dynamics of frontal cortex ensembles during memory-guided decision-making. PLoS Comput Biol 7:e1002057.

Bermudez-Rattoni F (2014) The forgotten insular cortex: its role on recognition memory formation. Neurobiol Learn Mem 109:207–216.

Bi GQ, Poo MM (2001) Synaptic modification by correlated activity: Hebb's postulate revisited. Annu Rev Neurosci 24:139–166.

Buzsáki G (1996) The hippocampo-neocortical dialogue. Cereb Cortex 6:81–92.

Dudai Y (2002) Molecular bases of long-term memories: a question of persistence. Curr Opin Neurobiol 12:211–216.

Dudai Y (2004) The neurobiology of consolidations, or, how stable is the engram? Annu Rev Psychol 55:51–86.

Eichenbaum H (2000) A cortical-hippocampal system for declarative memory. Nat Rev Neurosci 1:41–50.

Ferreira G, Gutiérrez R, De La Cruz V, Bermúdez-Rattoni F (2002) Differential involvement of cortical muscarinic and NMDA receptors in short- and long-term taste aversion memory. Eur J Neurosci 16:1139–1145.

Garcia J, Kimeldorf DJ, Koelling RA (1955) Conditioned aversion to saccharin resulting from exposure to gamma radiation. Science 122:157–158.

Grewe BF, Gründemann J, Kitch LJ, Lecoq JA, Parker JG (2017) Neural ensemble dynamics underlying a long-term associative memory. Nature 543:670–675.

Grossman SA, Fontanini A, Wieskopf JS, Katz DB (2008) Learning-related plasticity of temporal coding in simultaneously recorded amygdala–cortical ensembles. J Neurosci 28:2864–2873.

Haubrich J, Bernabo M, Baker AG, Nader K (2020) Impairments to consolidation, reconsolidation, and long-term memory maintenance lead to memory erasure. Annu Rev Neurosci 43:297–314.

Hopfield JJ (1982) Neural networks and physical systems with emergent collective computational abilities. Proc Natl Acad Sci U S A 79:2554–2558.

Jezzini A, Mazzucato L, La Camera G, Fontanini A (2013) Processing of hedonic and chemosensory features of taste in medial prefrontal and insular networks. J Neurosci 33:18966–18978.

Jones LM, Fontanini A, Sadacca BF, Miller P, Katz DB (2007) Natural stimuli evoke dynamic sequences of states in sensory cortical ensembles. Proc Natl Acad Sci U S A 104:18772–18777.

Kemere C, Santhanam G, Yu BM, Afshar A, Ryu SI, Meng TH, Shenoy K V (2008) Detecting neural-state transitions using hidden Markov models for motor cortical prostheses. J Neurophysiol 100:2441–2452.

Klinzing JG, Niethard N, Born J (2019) Mechanisms of systems memory consolidation during sleep. Nat Neurosci 22:1598–1610.

Laviolette SR, Lipski WJ, Grace AA (2005) A subpopulation of neurons in the medial prefrontal cortex encodes emotional learning with burst and frequency codes through a dopamine D_4 receptor-dependent basolateral amygdala input. J Neurosci 25:6066–6075.

Li Y, Zhou W, Li X, Zeng S, Liu M, Luo Q (2007) Characterization of synchronized bursts in cultured hippocampal neuronal networks with learning training on microelectrode arrays. Biosens Bioelectron 22:2976–2982.

Lubow RE (1973) Latent inhibition. Psychol Bull 79:398–407.

Lubow RE (2009) Conditioned taste aversion and latent inhibition: a review. In: Conditioned taste aversion: behavioral and neural processes (Reilly S, Schachtman TR, eds), pp 37–57. Oxford, UK: Oxford UP.

Ma L, Wang DD, Zhang TY, Yu H, Wang Y, Huang SH, Lee FS, Chen ZY (2011) Region-specific involvement of BDNF secretion and synthesis in conditioned taste aversion memory formation. J Neurosci 31:2079–2090.

Martínez-Moreno A, Rodríguez-Durán LF, Escobar ML (2011) Late protein synthesis-dependent phases in CTA long-term memory: BDNF requirement. Front Behav Neurosci 5:61.

Mason RJ, Rose SPR (1988) Passive avoidance learning produces focal elevation of bursting activity in the chick brain: amnesia abolishes the increase. Behav Neural Biol 49:280–292.

Mazzucato L, Fontanini A, La Camera G (2015) Dynamics of multistable states during ongoing and evoked cortical activity. J Neurosci 35:8214–8231.

Miller P, Katz DB (2010) Stochastic transitions between neural states in taste processing and decision-making. J Neurosci 30:2559–2570.

Moguel-González M, Gómez-Palacio-Schjetnan A, Escobar ML (2008) BDNF reverses the CTA memory deficits produced by inhibition of protein synthesis. Neurobiol Learn Mem 90:584–587.

Monk KJ, Rubin BD, Keene JC, Katz DB (2014) Licking microstructure reveals rapid attenuation of neophobia. Chem Senses 39:203–213.

Moran A, Katz DB (2014) Sensory cortical population dynamics uniquely track behavior across learning and extinction. J Neurosci 34:1248–1257.

Mukherjee N, Wachutka J, Katz DB (2019) Impact of precisely-timed inhibition of gustatory cortex on taste behavior depends on single-trial ensemble dynamics. Elife 8:e45968.

Müller GE, Pilzecker A (1900) Experimentelle beiträge zur lehre vom gedächtniss. Z Psychol Ergänzungsbd I:1–300.

Musall S, Kaufman MT, Juavinett AL, Gluf S, Churchland AK (2019) Single-trial neural dynamics are dominated by richly varied movements. Nat Neurosci 22:1677–1686.

Okun M, Steinmetz NA, Cossell L, Iacaruso MF, Ko H, Barthó P, Moore T, Hofer SB, Mrsic-Flogel TD, Carandini M, Harris KD (2015) Diverse coupling of neurons to populations in sensory cortex. Nature 521:511–515.

Parker LA, Hills K, Jensen K (1984) Behavioral CRs elicited by a lithium- or an amphetamine-paired contextual test chamber. Anim Learn Behav 12:307–315.

Phillips MI, Norgren RE (1970) A rapid method for permanent implantation of an intraoral fistula in rats. Behav Res Methods Instrum 2:124.

Piette CE, Baez-Santiago M. a, Reid EE, Katz DB, Moran A (2012) Inactivation of basolateral amygdala specifically eliminates palatability-related information in cortical sensory responses. J Neurosci 32:9981–9991.

Ponce-Alvarez A, Nácher V, Luna R, Riehle A, Romo R (2012) Dynamics of cortical neuronal ensembles transit from decision making to storage for later report. J Neurosci 32:11956–11969.

Poo M, Pignatelli M, Ryan TJ, Tonegawa S, Bonhoeffer T, Martin KC, Rudenko A, Tsai L-H, Tsien RW, Fishell G, Mullins C, Gonçalves JT, Shtrahman M, Johnston ST, Gage FH, Dan Y, Long J, Buzsáki G, Stevens C (2016) What is memory? The present state of the engram. BMC Biol 14:40.

Rabiner LR (1989) A tutorial on hidden Markov models and selected applications in speech recognition. Proc IEEE 77:257–285.

Rolls ET (2010) Attractor networks. Wiley Interdiscip Rev Cogn Sci 1:119–134.

Rosenblum K, Meiri N, Dudai Y (1993) Taste memory: the role of protein synthesis in gustatory cortex. Behav Neural Biol 59:49–56.

Rossant C, Kadir SN, Goodman DFM, Schulman J, Hunter MLD, Saleem AB, Grosmark A, Belluscio M, Denfield GH, Ecker AS, Tolias AS, Solomon S, Buzsáki G, Carandini M, Harris KD (2016) Spike sorting for large, dense electrode arrays. Nat Neurosci 19:634–641.

Sadacca BF, Rothwax JT, Katz DB (2012) Sodium concentration coding gives way to evaluative coding in cortex and amygdala. J Neurosci 32:9999–10011.

Sadacca BF, Mukherjee N, Vladusich T, Li JX, Katz DB, Miller P (2016) The behavioral relevance of cortical neural ensemble responses emerges suddenly. J Neurosci 36:655–669.

Sherstinsky A (2020) Fundamentals of recurrent neural network (RNN) and long short-term memory (LSTM) network. Physica D 404:132306.

Spector AC, Breslin P, Grill HJ (1988) Taste reactivity as a dependent measure of the rapid formation of conditioned taste aversion: a tool for the neural analysis of taste-visceral associations. Behav Neurosci 102:942–952.

Squire LR, Alvarez P (1995) Retrograde amnesia and memory consolidation: a neurobiological perspective. Curr Opin Neurobiol 5:169–177.

Stringer C, Pachitariu M, Steinmetz N, Reddy CB, Carandini M, Harris KD (2019) Spontaneous behaviors drive multidimensional, brainwide activity. Science 364:6437.

Tye KM, Stuber GD, de Ridder B, Bonci A, Janak PH (2008) Rapid strengthening of thalamo-amygdala synapses mediates cue-reward learning. Nature 453:1253–1257.

Wu C-H, Ramos R, Katz DB, Turrigiano GG (2021) Homeostatic synaptic scaling establishes the specificity of an associative memory. Curr Bio 1: 1–12.

Xin J, Ma L, Zhang T-Y, Yu H, Wang Y, Kong L, Chen Z-Y (2014) Involvement of BDNF signaling transmission from basolateral amygdala to infralimbic prefrontal cortex in conditioned taste aversion extinction. J Neurosci 34:7302–7313.

Yamamoto T, Fujimoto Y (1991) Brain mechanisms of taste aversion learning in the rat. Brain Res Bull 27:403–406.

Yasoshima Y, Yamamoto T (1998) Short-term and long-term excitability changes of the insular cortical neurons after the acquisition of taste aversion learning in behaving rats. Neuroscience 84:1–5.

Yu B, Cunningham J, Santhanam G, Ryu S, Shenoy K, Sahani M (2009) Gaussian-process factor analysis for low-dimensional single-trial analysis of neural population activity. J Neurophysiol 102:614–635.

Ziv Y, Burns LD, Cocker ED, Hamel EO, Ghosh KK, Kitch LJ, El Gamal A, Schnitzer MJ (2013) Long-term dynamics of CA1 hippocampal place codes. Nat Neurosci 16:264–266.